# The dynamics of the non-heme iron in bacterial reaction centers from *Rhodobacter sphaeroides*

A. Hałas [a], A. Orzechowska [a], V. Derrien [b], A.I. Chumakov [c], P. Sebban [b,d], J. Fiedor [a], M. Lipińska [e], M. Zając [c], T. Ślęzak [a], K. Strzałka [f], K. Matlak [a], J. Korecki [a], L. Fiedor [f], K. Burda [a,*]

[a] *AGH University of Science and Technology, Faculty of Physics and Applied Computer Science, al. Mickiewicza 30, 30-059 Kraków, Poland*
[b] *Laboratoire de Chimie Physique, CNRS UMR80000, Bat. 350, University of Paris-Sud, 91 405 Orsay, France*
[c] *European Synchrotron Radiation Facility, 6 rue J. Horowitz BP220, 38 043 Grenoble Cedex 9, France*
[d] *University of Science and Technology of Hanoi, 18 Hoang Quoc Viet, Cau Giay, Hanoi, Vietnam*
[e] *Arcan Institute, ul. Płukownika Dąbka, 30-732 Kraków, Poland*
[f] *Faculty of Biochemistry, Biophysics and Biotechnology, Jagiellonian University, ul. Gronostajowa 7, 30-387 Kraków, Poland*

ABSTRACT

We investigate the dynamical properties of the non-heme iron (NHFe) in His-tagged photosynthetic bacterial reaction centers (RCs) isolated from *Rhodobacter* (*Rb.*) *sphaeroides*. Mössbauer spectroscopy and nuclear inelastic scattering of synchrotron radiation (NIS) were applied to monitor the arrangement and flexibility of the NHFe binding site. In His-tagged RCs, NHFe was stabilized only in a high spin ferrous state. Its hyperfine parameters (IS = $1.06 \pm 0.01$ mm/s and QS = $2.12 \pm 0.01$ mm/s), and Debye temperature ($\theta_{D0} \sim 167$ K) are comparable to those detected for the high spin state of NHFe in non-His-tagged RCs. For the first time, pure vibrational modes characteristic of NHFe in a high spin ferrous state are revealed. The vibrational density of states (DOS) shows some maxima between 22 and 33 meV, 33 and 42 meV, and 53 and 60 meV and a very sharp one at 44.5 meV. In addition, we observe a large contribution of vibrational modes at low energies. This iron atom is directly connected to the protein matrix via all its ligands, and it is therefore extremely sensitive to the collective motions of the RC protein core. A comparison of the DOS spectra of His-tagged and non-His-tagged RCs from *Rb. sphaeroides* shows that in the latter case the spectrum was overlapped by the vibrations of the heme iron of residual cytochrome $c_2$, and a low spin state of NHFe in addition to its high spin one. This enabled us to pin-point vibrations characteristic for the low spin state of NHFe.

© 2012 Elsevier B.V. All rights reserved.

## 1. Introduction

The photosynthetic reaction center (RC) from *Rhodobacter sphaeroides* (*Rb. sphaeroides*), a non-sulfur purple bacterium, is a convenient model system for studying the dynamical and structural proprieties of type II photosynthetic RCs. The core of this RC consists of three protein subunits, L, M and H. The subunits L and M bind several bacteriochlorophyll (BChl) and bacteriopheophytin (BPheo) molecules. On the acceptor side, the polypeptides are connected via the non-heme iron (NHFe) which is symmetrically situated between the primary and secondary ubiquinone

acceptors $Q_A$ and $Q_B$, respectively. The ubiquinones are separated about 18 Å from each other. NHFe is a very conservative component of type II RCs [1]. Together with the two ubiquinones it forms a quinone–iron complex ($Q_A$–Fe–$Q_B$). The X-ray studies show that in RCs isolated from *Rb. sphaeroides* NHFe is hexacoordinated and its ligands form a distorted-octahedral environment [2,3]. NHFe is ligated by nitrogen atoms of the imidazole moiety of four histidine (His) residues. Two of these residues belong to the L subunit (L190 and L230) and the other two are bound to the M subunit (M219 and M266). The two other ligands are oxygen atoms from the M234 glutamine amino acid. The NHFe role in photosynthetic charge separation and in the temperature activation of electron transfer (ET) between $Q_A$ and $Q_B$ ubiquinones remains unclear [4–6]. No change in the NHFe valence state was observed in native type II RCs, which usually occurs in a high spin ferrous state [7–9]. However, in native photosynthetic systems isolated from algae and purple bacteria, two spin states of $NHFe^{2+}$ were detected [10,11]. In particular, the RCs isolated from *Rb. sphaeroides* contained NHFe in the high (HS) and low (LS) spin ferrous states while for the RCs from *Rhodospirillum* (*Rs.*) *rubrum*, NHFe occurred almost exclusively in the low spin state [10]. Recently, a correlation between the spin state and

iron vibrational properties was found [10]. In particular, it was shown that the occurrence of the low spin state resulted in a diminishment of vibrational modes at low energies between 2 and 8 meV (acoustic modes) and at higher energies (27–28.5 meV), and in an enhancement of modes between 10.5 and 26 meV.

In this paper, we concentrate on the comparison of NHFe properties in non-His-tagged RCs and in high purity His-tagged RCs isolated from bacteria *Rb. sphaeroides* grown under different lighting conditions. To investigate in detail the valence and spin state of NHFe we have applied [57]Fe-Mössbauer spectroscopy, one of the most powerful and sensitive tools for studying the state of iron atoms. The temperature dependent measurements provide us with valuable information on the flexibility of the NHFe binding site, as concluded from the mean square displacements of the iron atom. Detailed information on NHFe vibrations was obtained from the nuclear inelastic scattering (NIS) of synchrotron radiation. This unique method, which is complementary to Mössbauer spectroscopy, allowed us, for the first time, to obtain a pure spectrum of vibrational density of states (DOS) for the high spin NHFe ferrous state in His-tagged RCs. In these studies, the iron atom is a local sensor of the rigidity of the NHFe direct bonds as well as of the flexibility of the protein matrix in the vicinity of NHFe.

## 2. Materials and methods

### 2.1. Bacterial cultivation

Non-His-tagged *Rb. sphaeroides* bacterium was grown under anaerobic conditions in white light at 27 °C in a modified Hutner medium [12] supplemented with the iron isotope [57]Fe. The cells were harvested by centrifugation (6000 *g*, 20 min).

The cells of the *Rb. sphaeroides* bacterium carrying His-tagged mutation were grown in Erlenmeyer flasks filled to 50% of the total volume with a malate-yeast medium supplemented with kanamycin (20 μg/mL) and tetracycline (1.25 μg/mL). The medium was deprived of natural iron and enriched with [57]Fe. The cultures were grown in darkness at 30 °C on a gyratory shaker at 100 rpm. The cells were harvested by centrifugation (5000 *g*, 10 min).

To construct the WT His-tagged RCs, a sequence coding for 7 histidines was added at the 3′ terminus of the M subunit gene. This C-terminal extension facilitates a rapid and efficient recovery of purified RCs using immobilized metal affinity chromatography [13]. The plasmid used was PRK404 [14], carrying pufQBALMX [15].

### 2.2. Biochemical techniques

The purification of the non-His-tagged WT RC has previously been described in [10]. Cells from the His-tagged WT strain were disrupted by sonication in a 10 mM Tris HCl (pH 8) and 100 mM NaCl buffer. The resulting solution was centrifuged for 10 min at 10,000 *g*. Membrane solubilization was done by adding lauryldimethylamine *N*-oxide (LDAO; Fluka) to a final concentration of 0.8% in dark conditions with the presence of 8 mM imidazole. After ultrasonication (40,000 rpm for 75 min), the RCs were incubated in 40 mL of Ni Superflow pre-equilibrated with a 10 mM Tris HCl pH 8 and 0.1% LDAO buffer. The solubilized RCs were purified on a nickel affinity column and eluted with a buffer containing 10 mM Tris HCl pH 8, 0.1% LDAO and 40 mM imidazole. The bacterial RCs were concentrated using a micro-concentrator (Vivaspin, MWCO 30 kDa). As calculated from the measured absorbance at 802 nm [16] we obtained 890 nmol of BRCs.

No cryo-protectants were used in the low-temperature experiments. For the Mössbauer experiments the samples were frozen in liquid nitrogen, whereas for the NIS measurements they were lyophilized because of the experimental limitations of the sample volume. All samples were kept in darkness.

### 2.3. Mössbauer spectroscopy

The Mössbauer [57]Fe spectra were recorded in a homemade cryostat using 50 mCi [57]Co/Rh as a source of 14.4 keV radiation, and a proportional counter was used for detection purposes. A temperature within the range of 80 to 260 K was stabilized within 0.1 K. The recorded spectra were fitted using a recoil program [17]. The isomer shifts are given vs. metallic Fe at room temperature.

From the theoretical evaluation of the Mössbauer spectra one obtains the values of the hyperfine parameters, i.e. an isomer shift (IS) and a quadrupole splitting (QS), which are very sensitive to the chemical surrounding of the probing atom [18]. Electric monopole interactions between the nucleus and the electrons alter the energy separation between the ground state and the excited state of the Fe nucleus, thereby causing a slight shift in the position of the resonance line. The shift depends on the chemical environment of the Fe nucleus. In practice the nuclear term is a constant for a given transition and therefore for chemical application Eq. (1) is important.

The isomer shift is a measure of the difference between the electron density at the source nucleus $\sum_S |\phi(0)|^2$ and at the absorber nucleus $\sum_A |\phi(0)|^2$:

$$IS = K\left\{\sum_A |\phi(0)|^2 - \sum_S |\phi(0)|^2\right\}, \tag{1}$$

where K is the constant nuclear term. The s-electron density inside the [57]Fe nucleus is affected by the screening effects of d-electrons, and by covalency and bond formation, i.e. by the chemical bonding of the iron atom. Because ferrous iron has a lower electron density at the nucleus than does ionic ferrous iron, the isomer shift in ionic ferrous materials tends to lie within a range from 0.7 mm/s to 1.4 mm/s. However, LS spin iron in ferrous compounds is characterized by a small isomer shift, lower than 0.4 mm/s, due to the increased covalent character of the bonds in a strong electric field gradient.

Electric quadrupole interactions generate multiple-line spectra. Any nucleus with a spin quantum number I > 1/2 has a non-spherical charge distribution, which contains a quadrupole term eQ. In a chemically bonded atom, the electrostatic charge distribution is not usually spherically symmetric and therefore the interaction between the nuclear quadrupole moment and the electric field gradient (eq) results in energy level splitting. The excited nuclear state of iron [57]Fe with a nuclear spin I = 3/2 separates into two sublevels $|I = 3/2, \pm 3/2\rangle$ and $|I = 3/2, \pm 1/2\rangle$ whereas the ground level $|I = 1/2, \pm 1/2\rangle$ remains unsplit. Definite selection rules allow only transitions for $[I_{ze} - I_{zg}] = m = 0, \pm 1$ and thus the resultant spectrum comprises two lines of equal intensities for an isotropic powder/frozen sample. The energy separation, QS, between the two lines is equal to:

$$QS = \left|\frac{e^2qQ}{2}\right|. \tag{2}$$

Because eQ is a nuclear constant for a given Mössbauer probe, quadrupole splitting is a function of eq, so it is a function of the chemical environment. The electric field gradient is a negative second derivative of the potential at the nucleus of the whole surrounding electric charge, in which the valence electrons of the iron atom and surrounding ions contribute. If one ignores the effects of spin-orbit coupling, one can make a general prognosis about the expected quadrupole interaction. In the HS ferrous case, in addition to a spherically symmetric subshell, a single electron in the xy state is present. This electron provides an asymmetric charge distribution and will give rise to a large quadrupole interaction. In the LS ferrous case the electrons completely fill the lower triplet, the charge distribution has cubic symmetry, and no quadrupole interaction with the nucleus will result from it. However, one may expect a small contribution from the remote charges of the ligands and the more distant atoms.

Therefore, the values of hyperfine parameters obtained from the experimental spectra are "finger-prints" of the respective binding sites of the Fe atom.

## 2.4. Nuclear inelastic scattering of synchrotron radiation

The nuclear inelastic scattering of synchrotron radiation measurements was performed at the Nuclear Resonance Beamline ID 18 [19] at the European Synchrotron Radiation Facility in Grenoble, France operating in 16 bunch mode. The energy was tuned around the $^{57}$Fe transition energy of 14.412 keV with a resolution of 0.8 meV. NIS spectra were collected within an energy range from −40 to 100 meV and from −20 to 80 meV for non-His-tagged and His-tagged RCs, respectively. The measurements were done at a temperature of 60 K. A statistically meaningful spectrum of iron vibration modes in RCs was obtained after 10–12 h of data collection for non-His-tagged RCs, whereas the spectrum of His-tagged RCs was collected over 24 h. More details on the experimental method and setup are described in [19,20].

DOS is calculated from the inelastic part of the normalized NIS spectra after subtraction of the elastic contribution using the instrumental function measured in parallel and a procedure based on Lipkin's sum rule [21–23]. The data processing was performed using a double-Fourier transformation routine described in Ref. [24]. The normalized probability of inelastic nuclear absorption W(E) can be decomposed in multiphonon terms [25]:

$$W(E) = f_{LM}\left(\delta(E) + \sum_{n=1}^{\infty} S_n(E)\right). \quad (3)$$

$\delta(E)$ is a zero-phonon term, describing the elastic part of the absorption, and $S_n(E)$ is the inelastic absorption accompanied by the creation or annihilation of n phonons. The one phonon term is given by:

$$S_1(E) = \frac{E_R \cdot g(|E|)}{E \cdot \left(1 - e^{-\frac{E}{k_BT}}\right)}, \quad (4)$$

and the n-term in the harmonic approximation by:

$$S_n(E) = \frac{1}{n} \int_{-\infty}^{\infty} S_1\left(E'\right) S_{n-1}\left(E - E'\right) dE', \quad (5)$$

where $E_R = \frac{\hbar^2 k^2}{2m}$ is the recoil energy of a free nucleus, m is the mass of the atom and k is the wave vector of the X-ray quantum. The function g(E) is a normalized partial DOS, which assumes an averaging over all crystallographic directions.

## 3. Results and discussion

Our aim was to compare the properties of NHFe in high purity His-tagged and non-His-tagged RCs isolated from *Rb. sphaeroides* cells grown in darkness and under white light conditions, respectively. The purity of the His-tagged RCs was analyzed electrophoretically by SDS-PAGE, showing only the presence of the L, M and H polypeptides (Fig. 1A). Additionally, as shown in Fig. 1B, the absorption spectrum of the His-tagged RCs indicates a high protein-to-BChla ratio. The integrity of the His-tagged RCs was confirmed by the absorption spectra and their photochemical activity under strong illumination (reversible photobleaching of the P860 band, not shown) both before and after the Mössbauer and NIS experiments. The freeze-dried samples showed a complete recovery of their activity after rehydration at the room temperature (not shown). A similar characterization of the non-His-tagged RCs of *Rb. sphaeroides* was performed previously (Supplementary materials in [10]). In the case of the non-His-tagged RCs a small amount of residual cytochrome (cyt) c2 in addition to the three main proteins was detected based on SDS-PAGE and Mössbauer spectroscopy [10].

## 3.1. Mössbauer measurements

We applied Mössbauer spectroscopy to study the chemical and dynamical properties of NHFe in highly purified His-tagged RCs of *Rb. sphaeroides*. We compare the obtained hyperfine parameters and mean square displacement of NHFe to the data previously detected for non-His-tagged RCs isolated from *Rb. sphaeroides* [10].

The exemplary Mössbauer spectra measured at 85 K are presented in Fig. 2. The spectra of His-tagged RCs (Fig. 2B) were fitted using a single symmetric doublet of two Lorentzian lines. In the case of non-His-tagged RCs a superposition of four symmetric doublets was necessary to get a good quality fit (Fig. 2A). The line widths of the components of non-His-tagged and His-tagged bacterial RCs of about $0.18 \pm 0.01$ mm/s and $0.23 \pm 0.03$ mm/s, respectively, indicate high homogeneity of the iron binding sites. Thus in the His-tagged RCs we observe a single iron binding site with an isomer shift of about 1.06 mm/s and quadrupole splitting of about 2.12 mm/s at 85 K (Figs. 2B and 3A and B). These hyperfine parameters are characteristic for a high spin (HS) reduced ferrous NHFe. In the spectra of non-His-tagged RCs (Fig. 2A) two components can be assigned to two heme-iron (HFe) states in residual cyt. c. Both HFes are in the low spin (LS) ferrous state if one assumes that the component with a quadrupole splitting of about 2.0 mm/s and a small isomer shift of about 0.1 mm/s originates from the HFe ligated to the oxygen molecule [10]. The second HFe component has IS ≈ 0.3 mm/s and QS ≈ 1.0 mm/s. The other two subspectra come from NHFe, which exists both in a high and a low spin ferrous state and they contribute almost equally to the spectra of non-His-tagged RCs (Fig. 2A). The NHFe components characterized by IS ≈ 0.3 mm/s and QS ≈ 0.5 mm/s and by IS ≈ 1.05 mm/s and QS ≈ 2.1 mm/s at 85 K (Figs. 2A and 3) are assigned to the LS and HS states of reduced iron, respectively. Such a diamagnetic state (LS ferrous state) of NHFe has already been observed in other native photosynthetic systems of type II [10,11].

As the main focus here is the comparison of NHFe states between the two strains of *Rb. sphaeroides*, in Fig. 3A and B, the temperature dependence of the HFe hyperfine parameters is not analyzed at present (the respective data are reported in [10]). The perfect coincidence of the temperature dependence of the isomer shift and quadrupole splitting values of the NHFe HS state, observed in non-His-tagged and His-tagged RCs grown under different light conditions, shows that the first coordination sphere of NHFe in the $Q_A$–Fe–$Q_B$ complex is the same for both *Rb. sphaeroides* strains. The reason for the occurrence of the LS state of NHFe in the case of the non-His-tagged RCs is not clear, but we suggest that modifications of the hydrogen network in the vicinity of the $Q_A$–Fe–$Q_B$ complex may be responsible for the NHFe spin state changes. The importance of the H-bonds in stabilizing the spin state of NHFe was already confirmed by studies of the RCs from *Rs. rubrum* [10] and photosystem II of the *Chlamydomonas reinhardtii* PSI minus mutant, either untreated or treated with α-tocopheroquinone or copper ions [11,25]. The change from a bidentate to a monodentate coordination of the bicarbonate in NHFe in photosystem II or of the carboxyl group of a glutamate M-Glu234 in *Rb. sphaeroides* was also indicated as one of the mechanisms which may influence the NHFe spin state [26]. Moreover, our recent Mössbauer studies on the His-tagged RCs of *Rb. sphaeroides* with a triple mutation showed that the hydrophobicity of the $Q_A$ binding site can be crucial to the stabilization of NHFe in the HS ferrous state [27]. However, it cannot be ruled out that in the case of the non-His-tagged RCs the presence of cyt. c could result in a structural rearrangement of the core polypeptides, e.g. via allosteric interactions, thus causing modification of the protein surrounding of the iron–quinone complex and finally the formation of a LS $Fe^{2+}$ state.
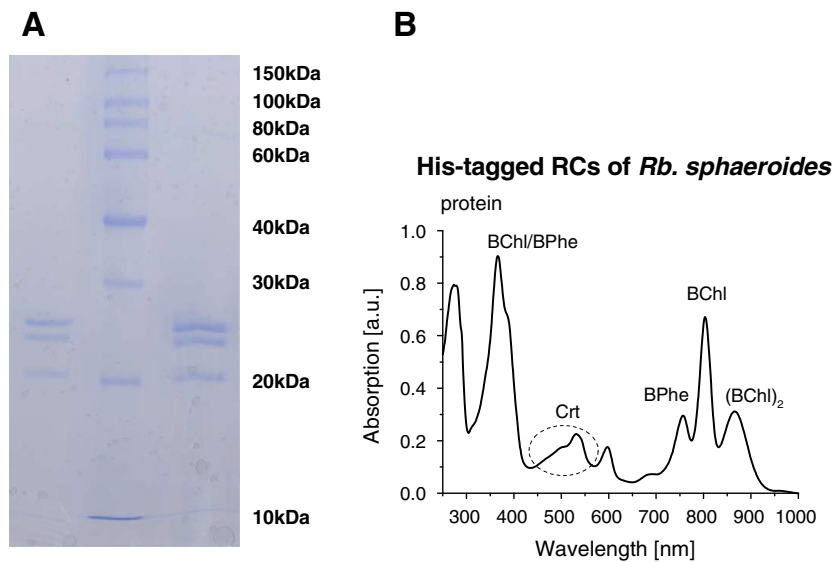
**Fig. 1.** (A) Electrophoretic analysis (SDS-PAGE) of the polypeptide composition of reaction centers from His-tagged RCs of *Rb. sphaeroides* (left and right lines show the two different concentrations of the sample, about 20 and 15 μM of BRCs, respectively). The middle line is a protein mass marker. The electrophoresis was done according to Laemmli U. K. (Nature 1970, 227, 680–685) using a 13% gel. (B) Absorption spectrum of His-tagged RCs of *Rb. sphaeroides*. Symbols: (BChl)2 — bacteriochlorophyll dimer (special pair); BChl — bacteriochlorophyll monomer; BPhe — bacteriopheophytin; Crt — carotenoids.

Temperature dependent measurements allow us also to get an insight into the flexibility of the NHFe binding site and especially to compare the dynamical properties of the NHFe HS state in the non-His-tagged and His-tagged RCs of *Rb. sphaeroides*. The mean square displacement $<x^2>$ of NHFe was calculated using the Lamb–Mössbauer factor, $F_{LM}$:

$$F = S \cdot F_{LM} = S \cdot \exp\left(-k^2 \left\langle x^2 \right\rangle\right), \tag{6}$$

where k is a wave number equal to $k = 2\pi E_\gamma/hc = 1/0.137 \ Å^{-1}$ for the Mössbauer transition of 14.4 keV in $^{57}$Fe; S is a proportionality factor. The $<x^2>$ value was normalized by extrapolation to 0 at a temperature of 0 K according to the classical approach. The mean square displacement at a low temperature approximation is well described by the Debye model (below 160 K). At higher temperatures, collective motions from the protein matrix become more important than fast vibrational motions [28–30]. In this case anharmonic corrections to the Debye model have to
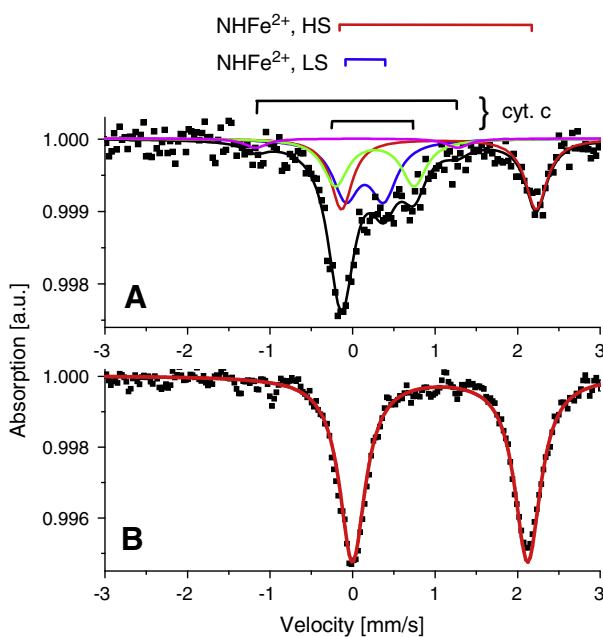


**Fig. 2.** Mössbauer spectra of non-His-tagged reaction centers (RCs) [10] (A) and His-tagged RCs (B) isolated from *Rb. sphaeroides*. The filled squares represent the experimental data. The solid lines represent fits assuming symmetrical Lorentzian lines. Different components are indicated by various colors. The spectra were measured at T = 85 K. The line width was 0.18 ± 0.01 mm/s for His-tagged and about 0.23 ± 0.03 mm/s in non His-tagged RCs.
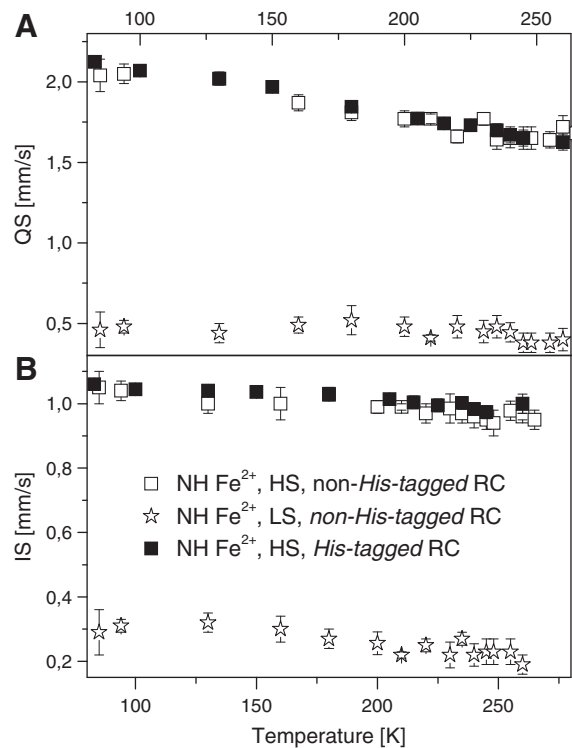


**Fig. 3.** The temperature dependence of hyperfine parameters of NHFe fitted to the Mössbauer spectra of non-His-tagged (open symbols) and His-tagged (closed symbols) RCs of *Rb. sphaeroides*. IS — isomer shift (A), QS — quadrupole splitting (B).

be taken into account. A first approximation of the Debye temperature was made:

$$\theta_D = \theta_{D0}(1 + AT + \ldots), \tag{7}$$

where $\theta_{D0}$ is the Debye temperature from a low temperature approximation, A is a parameter of the effective Debye temperature variation and T is the absolute temperature [11,31]. The experimentally obtained $<x^2>$ of NHFe in the His-tagged and non-His-tagged bacterial RCs is shown in Fig. 4. The solid lines present theoretical fits and the fitted parameters are collected in Table 1.

The Debye temperature characterizing the flexibility of NHFe in His-tagged RCs is similar to the one estimated for the high spin state of NHFe in non-His-tagged RCs. This confirms that not only the chemical properties (see hyperfine parameters in Fig. 3), but also the dynamical properties of NHFe binding sites, are similar in both RCs when the iron atom is in a HS reduced state. For HS ferrous NHFe, the Debye temperature from a low temperature approximation is about 166 K, which is much lower than that one obtained for the low spin NHFe in non-His-tagged RCs ($\theta_{D0} \sim 207$ K). The Debye temperature is related to the solid-state vibrations of NHFe. Its value entirely determines the temperature dependence of the NHFe mean square displacement below $\theta_{D0}$, which is linear. Therefore one may estimate an effective mean force constant f from the slope of the linear part of $<x^2>$, as proposed in [32]:

$$\left\langle x^2 \right\rangle = \frac{k_B}{f_v} T, \tag{8}$$

where $k_B$ is the Boltzmann constant equal to $1.38 \times 10^{-23}$ J/K. For less rigid NHFe the average value of the force constant of the iron–ligand bond should be smaller. For the HS state of NHFe in both bacterial RCs we found this constant to be $f_v \approx 20$ N/m whereas for the LS state of NHFe observed in non-His-tagged RCs $f_v \approx 46$ N/m. These force constant values are an order of magnitude higher than those calculated from the slope of the average mean square displacement of the atoms composing the RC protein matrix as a function of the temperature obtained for His-tagged RCs of *Rb. sphaeroides* in neutron scattering experiments within a temperature range from 20 K to 130 K [33]. The reason for this difference is that in Mössbauer measurements the solid state vibrations are determined mainly by the strength of the iron bonds from its first coordination sphere, whereas in neutron scattering
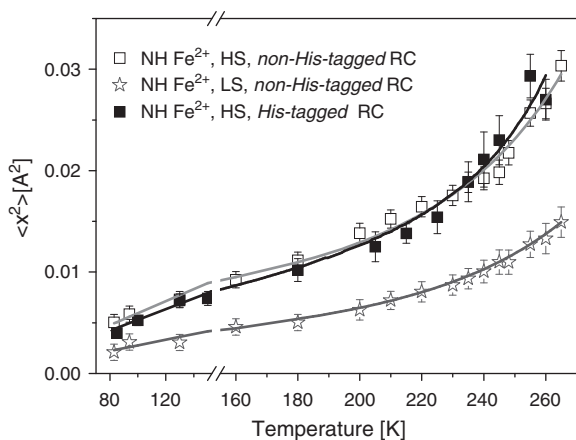
### Table 1
Debye temperature at a low temperature approximation $\theta_{D0}$ and the A parameter describing the linear variation of $\theta_D$ with temperature evaluated from the fits of the experimental data shown in Fig. 4.

| Parameter | HS NHFe in His-tagged RCs | HS NHFe in non-His-tagged RCs | LS NHFe in non-His-tagged RCs |
|---|---|---|---|
| $\theta_{D0}$ [K] | $166 \pm 19$ | $168 \pm 18$ | $207 \pm 12$ |
| A [1/K] | $-0.0031 \pm 0.0001$ | $-0.0028 \pm 0.0002$ | $-0.0031 \pm 0.0001$ |

HS — high spin; LS — low spin.

experiments the dominant contribution comes from the hydrogen motions of the protein sidechains [34].

At temperatures higher than $\theta_{D0}$, the mean square displacement of NHFe shows a deviation from linearity, which means that it increases much faster than the Debye model predicts (see Fig. 4). Within the studied range of temperatures the anharmonicity comes from the activated fast and slow collective motions of the protein matrix in the NHFe surrounding [30]. This means that at $T > \theta_{D0}$ in formula (8) the value of the mean force constant f comes not only from iron bonds $f_v$, but also from the protein bonds from more distant places of the RC core, which makes NHFe sense its binding site as softer at higher temperatures. It is known that NHFe direct bonds are the strongest among all other bonds in bacterial RCs [33], and that is why the increased flexibility of its binding site observed in Mössbauer experiments is due to the decreased effective mean force constant $f_{eff}$, which should replace $f_v$ in Eq. (8). Within a certain range of temperatures the radius of the NHFe further protein coordination sphere, influencing the iron binding site, increases with increasing temperature up to a certain distance, at which protein flexibility does not change the effective mean force constant any more. So for large temperatures the dependence $<x^2>$ (T) again becomes linear but with a much higher slope than that observed for $T < \theta_{D0}$. Thus, in this case one can assume that the effective average force constant can be expressed as:

$$\frac{1}{f_{eff}} = \frac{1}{f_v} + \frac{1}{f_{col}}, \tag{9}$$

where $f_{col}$ (we will call it the collective force constant) is the effective average force constant of the protein matrix, i.e. of all bonds starting from the 2nd ($f_2$), 3rd ($f_2$), … and nth ($f_n$) coordination sphere and

$$\frac{1}{f_{col}} = \sum_{i=2}^{n} \frac{1}{f_i}, \tag{10}$$

while $f_1 = f_v$.

From the experimental data presented in Fig. 4 we estimated that $f_{col} \approx 2.0$ N/m and 2.7 N/m for the HS state of NHFe in His-tagged and non-His-tagged RCs, respectively, and $f_{col} \approx 6.6 \pm 0.1$ N/m for the NHFe LS state detected in the case of non-His-tagged RCs. These values suggest that the rigidity of the protein backbone is comparable for non-His-tagged and His-tagged RCs when NHFe is in the HS state but that it increases about 3-folds in the case of the iron LS state observed in non-His-tagged RCs of *Rb. sphaeroides*. Although dynamic studies using Mössbauer spectroscopy allow us to detect much slower motions (between 0.1 ns and 100 ns) than neutron spectroscopy (between 0.1 ps and 1 ns), it is important to note that the force constants $f_{col}$ calculated here are in a very good agreement with those obtained from neutron backscattering reported for the protein core of His-tagged RCs (3.8 N/m) in [33].

Temperature dependent Mössbauer studies of the solvent influence on the protein matrix relaxation [35] show that the transition of $<x^2>$ observed at the temperatures above $\theta_{D0}$, can be compared with a glass transition.



**Fig. 4.** The temperature dependence of the mean square displacements of NHFe in non-His-tagged (open symbols) [10] and His-tagged (closed symbols) RCs of *Rb. sphaeroides*. The solid gray lines and the black line represent theoretical fits to the experimental data of non-His-tagged and His-tagged data, respectively.

### 3.2. NIS measurements

Nuclear inelastic scattering is a method complementary to Mössbauer spectroscopy. It provides unique information on DOS for a given atom, in the present experiment [57]Fe. In Fig. 5 we compare DOS spectra of non-His-tagged (A) and His-tagged (B) RCs of *Rb. sphaeroides*. As discussed previously [10], the DOS spectrum of *Rb. sphaeroides* RCs containing mainly HS NHFe is very different from that one of *Rs. rubrum* dominated by LS NHFe. Moreover, in those DOS spectra of non-His-tagged RCs, there is also a contribution from HFe of cyt. c. For the first time a measured pure DOS spectrum of NHFe in a HS $Fe^{2+}$ state in His-tagged RCs of *Rb. sphaeroides*, presented in Fig. 5B, unambiguously shows characteristic vibrational modes of HS NHFe in bacterial RCs.

In order to better visualize the distinctions between the DOS spectra of non-His-tagged and His-tagged RCs of *Rb. sphaeroides*, in Fig. 5C the differential spectrum ((A)–(B)) is presented. This figure shows differences in vibrational characteristics of the HS and LS iron, in particular when a contribution from cyt. c to the spectrum of non-His-tagged RCs is taken into account. The HFe in cyt. c, regardless of whether bound to protein or not, contributes significantly to the DOS spectrum only at energies above 35 meV with a maximum at around 45 meV, and a rather featureless and silent energy region between 8 meV and 30 meV [23,36–38]. The vibrations originating from cyt. c are observed in Fig. 5C as an enhancement at about 43 meV. The other differences in DOS seen in Fig. 5C are related to the occurrence of the additional spin state of $NHFe^{2+}$, i.e. its low spin state, in non-His-tagged RCs. At low energies, the presence of a low spin state of NHFe is reflected in a decrease of vibrational DOS at the energies 1.5–17.5 meV accompanied with an increase at 17.5–22.0 meV (Fig. 5C). The other features of the differential spectrum underline the spin-state-specific character of the vibrations

in the range of 24 meV–40 meV, with relatively sharp DOS peaks, and HS specific vibrations at 56 meV–58 meV.

Special attention should be paid to DOS at low energies. This part of the spectrum reveals the density of inter-molecular modes, which can be also interpreted as a softening of the lattice, i.e. the protein matrix contribution to NHFe vibrations [39–41]. The present Mössbauer results, as discussed above (see Eqs. (8)–(10)), showed a higher flexibility of NHFe in a HS state for both non-His-tagged and His-tagged RCs of *Rb. sphaeroides* in comparison to NHFe in a LS state present only in non-His-tagged RCs of *Rb. sphaeroides* and that is why $\theta_{D0}$ is lower for the iron HS state than for the LS one. Because high spin NHFe is more sensitive to protein matrix motions in its surrounding one should expect a significant contribution from the vibrational acoustic modes at low energies in the DOS spectrum of high spin NHFe. This is indeed confirmed by a higher contribution of the vibrations in this range of energy in His-tagged than in non-His-tagged RCs of *Rb. sphaeroides* (Fig. 5C). This part of the DOS spectrum is characteristic of glass materials and proteins [40,42,43], where long range interactions due to cooperativity are present. A similar behavior is known as a boson peak, which correlates in the height and position with the distribution of force constants of an ensemble of weakly anharmonic oscillators [44,45]. The involvement of extended hydrogen bond networks in the cooperative function between distant sites in bacterial RCs has been discussed in [46]. Because large-scale global protein motions may occur even on a picosecond timescale [47,48] and the contribution of protein collective motions enhanced by the temperature in the Mössbauer experiments correspond to the long arranged interactions of NHFe with the protein core activated by the X-ray radiation at any temperature in the case of the NIS method one can interpret these data in a common framework. We suggest that the differences in the density of vibrations in Fig. 5C at 60 K at the low
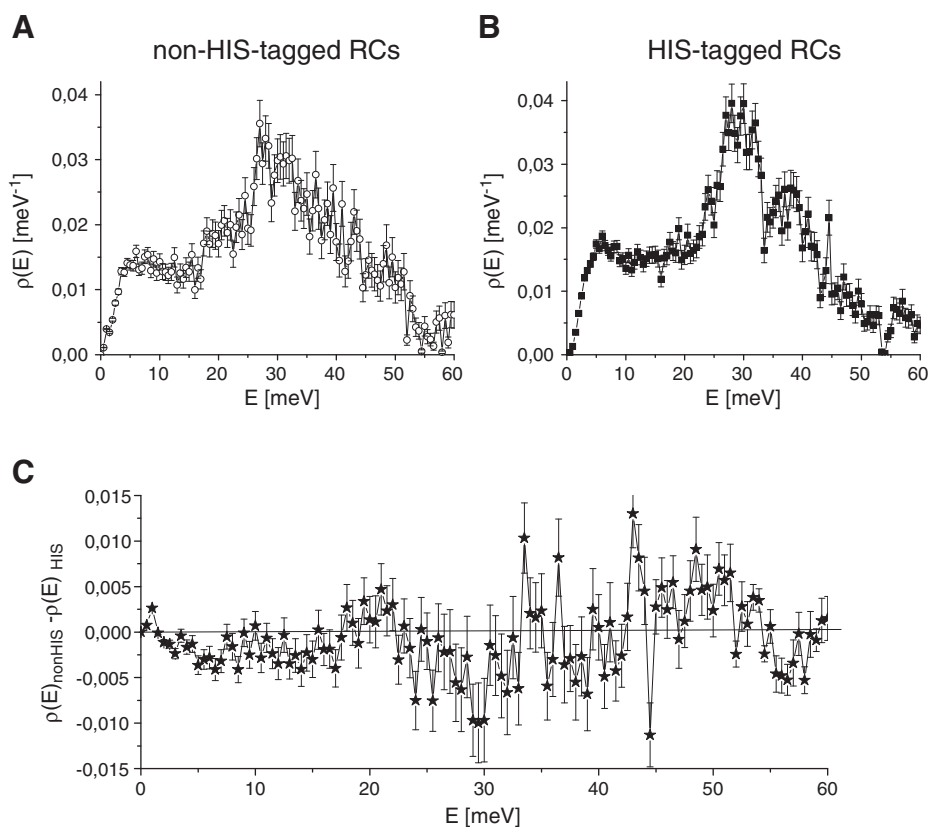


**Fig. 5.** Density of vibrational states (DOS), ρ(E), obtained from NIS experiments for (A) non-His-tagged RCs of *Rb. sphaeroides* containing cytochrome $c_2$ contaminations and NHFe in two different spin states [10] and (B) His-tagged RCs of *Rb. sphaeroides* in which NHFe occurs only in a high spin ferrous state. In (C) the difference between the two DOS spectra presented in (A) and (B) is shown. Measurements were performed at 60 K.

range of energies are caused by a higher softening of the NHFe binding site for the Fe high spin state (vide supra).

## 4. Conclusions

The Mössbauer-based studies of the non-heme iron (NHFe) in His-tagged RCs of *Rb. sphaeroides* grown in darkness show that NHFe is present only in a high spin ferrous state. Its hyperfine parameters are similar to those obtained for the high spin state of NHFe in non-His-tagged RCs of the bacterium grown in white light. Moreover, the flexibility of the NHFe binding site is comparable for both samples. The Debye temperature estimated for the high spin NHFe of these bacterial RCs is about $166 \pm 1$ K. We present here, for the first time, the vibrational modes of a pure high spin ferrous state of NHFe in a type II bacterial reaction center. The DOS spectrum shows a significant contribution of vibrations at low energies below 15 meV, which are related to the extreme sensitivity of NHFe to collective motions of the protein matrix in its vicinity. Because all ligands to NHFe are provided by the amino acids of the L and M proteins it is highly sensitive to surrounding protein fluctuations. Therefore, in contrast to heme-irons, this NHFe is characterized by vibrational modes whose main contribution is at energies below 35 meV.

The temperature dependent Mössbauer and photo-induced optical absorbance change measurements show that the activation of the collective motions at temperatures above the Debye temperature is crucial for activation of the electron transfer between the two external quinone electron acceptors $Q_A$ and $Q_B$ [49,50]. Moreover, the functioning of $Q_B$ was shown to be regulated by the flexibility and hydrogen network of its surrounding [2,51]. Because the DOS spectra reflect the NHFe state and the fluctuations of protein matrix coupled to it, we conjecture that the identified NHFe vibrational modes are good sensors for the proper photosynthetic activity of the bacterial RCs, especially of their acceptor side. The previous results obtained for RCs from *Rs. rubrum* and *Rb. sphaeroides* [10,52–54] support this hypothesis. In particular, energies below 10 meV are diminished in RCs of *Rs. rubrum* and consequently electron transfer on the acceptor side is less effective in these RCs than in those of *Rb. sphaeroides*. The long-range reactive dynamics which is pronounced in the low energy part of the DOS spectra is regulated mainly by hydrogen bonds and their capability for efficient rearrangement was shown to be crucial for proton uptake by the secondary quinone acceptor bound at the $Q_B$ site [1].

## References

[1] J. Koepke, E.-M. Krammer, A. Klingen, P. Sebban, G.M. Ullmann, G. Fritzsch, pH modulates the quinone position in the photosynthetic reaction center from *Rhodobacter sphaeroides* in the neutral and charge separated states, J. Mol. Biol. 371 (2) (2007) 396–409.
[2] J.P. Allen, G. Feher, T.O. Yeates, H. Komiya, D.C. Rees, Structure of the reaction center from *Rhodobacter sphaeroides* R-26: protein-cofactor (quinones and Fe$^{2+}$) interactions, Proc. Natl. Acad. Sci. U. S. A. 85 (1988) 8487–8491.
[3] In: J. Deisenhofer, J.R. Norris (Eds.), The Photosynthetic Reaction Center, Academic Press Inc., San Diego, 1993.
[4] D. Kleinfeld, M.Y. Okamura, G. Feher, Electron-transfer kinetics in photosynthetic reaction centers cooled to cryogenic temperatures in the charge-separated state: evidence for light-induced structural changes, Biochemistry 23 (1984) 5780–5786.
[5] L. Baciou, P. Sebban, Heterogeneity of the quinone electron-acceptor system in bacterial reaction centers, Photochem. Photobiol. 62 (2) (1995) 271–278.
[6] K. Burda, Dynamics of electron transfer in photosystem II, Cell Biochem. Biophys. 47 (2007) 271–284.

[7] S. Hermes, O. Bremm, F. Garczarek, V. Derrien, P. Liebisch, P. Loja, P. Sebban, K. Gerwert, M. Haumann, A time-resolved iron-specific X-ray absorption experiment yields no evidence for an Fe$^{2+}$ to Fe$^{3+}$ transition during $Q_A^-$ to $Q_B$ electron transfer in the photosynthetic reaction center, Biochemistry 45 (2006) 353–359.
[8] D. Kleinfeld, M.Y. Okamura, G. Feher, Electron transfer in reaction centers of *Rhodopseudomonas* sphaeroides. I. Determination of the charge recombination pathway of $D + QA \; QB - \cdot$ and free energy and kinetic relations between $QA - \cdot QB$ and $QA \; QB -$, Biochim. Biophys. Acta 766 (1984) 126–140.
[9] B. Boso, P. Debrunner, M.Y. Okamura, G. Feher, Mössbauer spectroscopy studies of photosynthetic reaction centers from *Rhodopseudomonas sphaeroides* R-26, Biochim. Biophys. Acta 638 (1981) 173–177.
[10] A. Orzechowska, M. Lipińska, J. Fiedor, A. Chumakov, M. Zając, T. Ślęzak, K. Matlak, K. Strzałka, J. Korecki, L. Fiedor, K. Burda, Coupling of collective motions of the protein matrix to vibrations of the non-heme iron in bacterial photosynthetic reaction centers, Biochim. Biophys. Acta 1797 (2010) 1696–1704.
[11] K. Burda, J. Kruk, R. Borgstadt, J. Stanek, K. Strzałka, G.H. Schmid, O. Kruse, Mossbauer studies of the non-heme iron and cytochrome b$_{559}$ in *Chlamydomonas reinhardtii* PSI$^-$ mutant and their interactions with a-tocopherol quinone, FEBS Lett. 533 (2003) 159–165.
[12] G. Cohen-Bazire, W.R. Sistrom, R.Y. Stanier, Kinetic studies of pigment synthesis by non-sulfur purple bacteria, J. Cell Comp. Physiol. 49 (1957) 25–58.
[13] J.O. Goldsmith, S.G. Boxer, Rapid isolation of bacterial photosynthetic reaction centers with an engineered poly-histidine tag, Biochim. Biophys. Acta 1276 (1996) 171–175.
[14] H.N. Scott, P.D. Laible, D.K. Hanson, Sequences of versatile, broad-host-range vectors of the RK2 family, Plasmid 50 (2003) 74–79.
[15] M.J. Hessner, P.J. Wejksnora, M.L. Collins, Construction, characterization, and complementation of *Rhodospirillum rubrum* puf region mutants, J. Bacteriol. 173 (18) (1991) 5712–5722.
[16] S.C. Straley, W.W. Parson, D.C. Mauzerall, R.K. Clayton, Pigment content and molar extinction coefficients of photochemical reaction centers, Biochim. Biophys. Acta 305 (1973) 597–609.
[17] D.G. Rancourt, J.-Y. Ping, Voigt-based methods for arbitrary-shape static hyperfine parameter distributions in Mössbauer spectroscopy, Nucl. Instr. Meth. B 58 (1991) 85–87.
[18] N.N. Greenwood, T.C. Gibb, Mössbauer Spectroscopy, in: Chapman and Hall Ltd., 1971, p. 650.
[19] R. Rüffer, A.I. Chumakov, Nuclear resonance beamline at ESRF, Hypertens. Interact. 589 (1996) 97–98.
[20] A.I. Chumakov, W. Sturhahn, Experimental aspects of inelastic nuclear resonance scattering, Hypertens. Interact. 123 (124) (1999) 781–808.
[21] H. Lipkin, Some simple features of the Mössbauer effect, Ann. Phys. 9 (1960) 332–339.
[22] H. Lipkin, Mössbauer sum rules for use with synchrotron sources, Phys. Rev. B 52 (1995) 10073–10079.
[23] K.L. Adams, S. Tsoi, J. Yan, S.M. Durbin, A.K. Ramdas, W.A. Cramer, W. Sturhahn, E.E. Alp, C. Schulz, Fe vibrational spectroscopy of myoglobin and cytochrome f, J. Phys. Chem. B 110 (2006) 530–536.
[24] V.G. Kohn, A.I. Chumakov, DOS: evaluation of phonon density of states from nuclear resonant inelastic absorption, Hypertens. Interact. 125 (2000) 205–221.
[25] K. Burda, J. Kruk, J. Stanek, K. Strzałka, G.H. Schmidt, O. Kruse, Mössbauer studies of Cu(II) ions with the non-heme iron and cytochrome b559 in *Chlamydomonas reinhardtii* PSI minus mutant, Acta Phys. Polon. A 109 (2006) 237–247.
[26] P. Cherniev, I. Zaharieva, H. Dau, M. Haumann, Carboxylate shift steer interquinone electron transfer in photosynthesis, J. Biol. Chem. 286 (2011) 5368–5374.
[27] A. Halas, V. Derrien, P. Sebban, K. Matlak, J. Korecki, J. Kruk, K. Burda, Chemical properties of the iron–quinone complex in mutated reaction centers of *Rb. sphaeroides*, Hypertens. Interact. 206 (2012) 109–114.
[28] M.H.B. Stowell, T.M. McPhillips, D.C. Rees, S.M. Soltis, E. Abresch, G. Feher, Light-induced structural changes in photosynthetic reaction center: implication for mechanism of electron–proton transfer, Science 276 (1997) 812–816.
[29] H. Frauenfelder, G.A. Petsko, T. Tsernoglou, Temperature-dependent X-ray diffraction as a probe of protein structural dynamics, Nature 280 (1997) 558–563.
[30] E.R. Bauminger, S.G. Cohen, I. Nowik, S. Ofer, J. Yariv, Dynamics of heme iron in crystals of metmyoglobin and deoxymyoglobin, Proc. Natl. Acad. Sci. U. S. A. 80 (1983) 736–740.
[31] K. Burda, A. Hrynkiewicz, H. Kołoczek, J. Stanek, K. Strzałka, Molecular dynamics and local electronic states of Sn and Fe in metallocytochrome and metalloporphyrin, Hypertens. Interact. 91 (1994) 891–897.
[32] D.J. Bicout, G. Zaccai, Protein flexibility from the dynamical transition: a force constant analysis, Biophys. J. 80 (2001) 1115–1123.
[33] S. Sacquin-Mora, P. Sebban, V. Derrien, B. Frick, R. Lavery, C. Alba-Simionesco, Probing the flexibility of the bacterial reaction center: the wild-type protein is more rigid than two site-specific mutants, Biochemistry 46 (2007) 14960–14968.
[34] N. Engler, A. Ostermann, N. Niimura, F.G. Parak, Hydrogen atoms in proteins: positions and dynamics, Proc. Natl. Acad. Sci. U. S. A. 100 (2003) 10243–10248.
[35] A. Huenges, K. Achterhold, F.G. Parak, Mössbauer spectroscopy in the energy and in the time domain, a crucial tool for the investigation of protein dynamics, Hypertens. Interact. 144 (145) (2002) 209–222.
[36] B.M. Leu, Y. Zhang, L. Bu, J.E. Straub, J. Zhao, W. Sturhahn, E. Alp, J.T. Sage, Resilience of the iron environment in heme proteins, Biophys. J. 95 (2008) 5874–5889.
[37] Y. Xiao, M.-L. Tan, T. Ichiye, H. Wang, Y. Guo, M. Smith, J. Meyer, W. Sturhahn, E. Alp, J. Zhao, Y. Yoda, S. Cramer, Dynamics of *Rhodobacter capsulatus* [2Fe–2S] ferredoxin VI and *Aquifex aeolicus* ferredoxin 5 via nuclear resonance vibrational spectroscopy (NRVS) and resonance Raman spectroscopy, Biochemistry 47 (2008) 6612–6627.

[38] T. Kakitani, H. Kakitani, A possible new mechanism of temperature dependence of electron transfer in photosynthetic systems, Biochim. Biophys. Acta 635 (1981) 498–514.

[39] J.T. Sage, S.M. Durbin, W. Sturhahn, D.C. Wharton, P.M. Champion, P. Hession, J. Sutter, E.E. Alp, Long-range reactive dynamics in myoglobin, Phys. Rev. Lett. 86 (2001) 4966–4969.

[40] K. Achterhold, C. Keppler, A. Ostermann, U. van Bürck, W. Sturhahn, E.E. Alp, F.G. Parak, Vibrational dynamics of myoglobin determined by the phonon-assisted Mössbauer effect, Phys. Rev. E 65 (2002) (051916-1–051916-13).

[41] A.I. Chumakov, R. Rüffer, O. Leupold, I. Sergueev, Insight to dynamics of molecules with nuclear inelastic scattering, Struct. Chem. 14 (2003) 109–119.

[42] K.G. Brown, S.C. Erfurth, E.W. Small, W.L. Peticolas, Conformationally dependent low-frequency motions of proteins by laser Raman spectroscopy, Proc. Natl. Acad. Sci. U. S. A. 69 (1972) 1467–1469.

[43] J. Pieper, T. Hauss, A. Buchsteiner, K. Baczyński, K. Adamiak, R.E. Lechner, G. Renger, Temperature- and hydration-dependent protein dynamics in photosystem II of green plants studied by quasielastic neutron scattering, Biochemistry 46 (2007) 11398–11409.

[44] T. Asthalter, M. Bauer, U. Van Bürck, I. Sergueev, H. Franz, A.I. Chumakov, Phonons in confinement and the boson peak using nuclear inelastic absorption, Hypertens. Interact. 144 (145) (2002) 77–83.

[45] A.I. Chumakov, G. Monaco, A. Monaco, W.A. Crichton, A. Bosak, R. Rüffer, A. Meyer, F. Kargl, L. Comez, D. Fioretto, H. Giefers, S. Roitsch, G. Wortmann, M.H. Manghnani, A. Hushur, Q. Williams, J. Balogh, K. Parliński, P. Jochym, P. Piekarz, Equivalence of the boson peak in glasses to the transverse acoustic van hove singularity in crystals, Phys. Rev. Lett. 106 (2011) (225501-1–225501-5).

[46] J. Tandori, L. Baciou, E. Aleksov, P. Maroti, M. Schiffer, D.K. Hanson, P. Sebban, Revealing the involvement of extended hydrogen-bond networks in the cooperative function between distant sites in bacterial reaction centers, J. Biol. Chem. 276 (2001) 45513–45515.

[47] L. Genberg, L. Richard, G. McLendon, D.R.J. Miller, Direct observation of global protein motion in hemoglobin and myoglobin on picosecond time scale, Science 251 (1991) 1051–1054.

[48] J. Deák, H.-L. Chiu, C.M. Lewis, D.R.J. Miller, Ultrafast phase grating studies of heme-proteins: observation of the low-frequency modes directing functionally important protein motions, J. Phys. Chem. B 998 (1998) 6621–6634.

[49] F. Parak, E.N. Frolov, A.A. Kononenko, R.L. Mössbauer, V.I. Goldanskii, A.B. Rubin, Evidence for a correlation between the photoinduced electron transfer and dynamic properties of the chromatophore membranes from *Rhodospirillum rubrum*, FEBS Lett. 117 (1980) 368–372.

[50] A. Garbers, F. Reifarth, J. Kurreck, G. Renger, F. Parak, Correlation between protein flexibility and electron transfer from QA$-^*$ to QB in PSII membrane fragments from spinach, Biochemistry 37 (1998) 11399–11404.

[51] B. Rabenstein, G.M. Ullmann, E.W. Knapp, Electron transfer between the quinones in the photosynthetic reaction center and its coupling to conformational changes, Biochemistry 39 (2000) 10487–10496.

[52] C.A. Wraight, Iron–quinone interactions in the electron acceptor region of bacterial photosynthetic reaction centers, FEBS Lett. 93 (1978) 283–288.

[53] P.D. Laible, Y. Zhang, A.L. Morris, S.W. Snyder, C. Ainsworth, S.R. Greenfield, M.R. Wasielewski, P. Parot, B. Schoepp, M. Schiffer, D.K. Hanson, M.C. Thurnauer, Spectroscopic characterization of quinone-site mutants of the bacterial photosynthetic reaction center, Photosynth. Res. 52 (1997) 93–103.

[54] P.H. McPherson, M.Y. Okamura, G. Feher, Electron transfer from the reaction center of *Rb. sphaeroides* to the quinone pool: doubly reduced QB leaves the reaction center, Biochim. Biophys. Acta 1016 (1990) 289–292.